Size-Based Rendering for Lung Cancer Screening

Rafael Wiemker, Thomas Bülow, Tobias Klinder

Philips Research Hamburg, Röntgenstrasse 24, 22335 Hamburg, Germany

Abstract

We present two relevant clinical use cases for thoracic computed tomography data, where the recently introduced concept of size-based rendering can be beneficially applied to medical visualization in the context of screening for lung cancer and chronic obstructive pulmonary disease (COPD):

(a) Gradual suppression of thorax and vessels for quick appraisal of the presence of pulmonary nodules.

(b) Visualization of bullous versus diffuse emphysema.

In the first use case, the opacity is chosen to decrease with local structure size, whereas in the second case, the opacity is chosen to increase with structure size. Both algorithms are robust in particular because they do not depend on any prior segmentation or classification. They are ideally suited for full parallelization and GPU implementation.

Categories and Subject Descriptors (according to ACM CCS): I.3.3 [Computer Graphics]: Picture/Image Generation—Display algorithms; J.3 [Life And Medical Sciences]: Medical information systems

1. Introduction and Related Work

In medical visualization, most practically used direct renderings of volumetric datasets (i.e. without prior object segmentation) use opacity transfer functions based on intensities, but also gradient- and curvature-based renderings have been explored [SWB*00, PSW*07, PB07, MJR08, WDB12, WKB*12]. More recently, size-based rendering has been introduced [CM08, HFRS*08, WK09, WKK10]. Here the rendering of each location depends not only on the local intensity but moreover also on the estimated size of the local structure. We present two clinical use cases related to screening for lung cancer and chronic obstructive pulmonary disease (COPD) which can profit significantly from the concept of size-based rendering.

Lung cancer screening with Computed Tomography (CT) is increasingly adopted after the overwhelming results of the recently concluded National Lung Cancer Screening Trial [Nat11, Coc12], and pulmonary nodules and emphysematic COPD are known to be the single most important indicators for developing lung cancer [SHA*07]. The most difficult task for the radiological reader is to differentiate lung nodules from normal surrounding vascular structures [Coc12]. Fully automated computer aided detection (CAD) of lung nodules and emphysema is being explored but is met with a certain skepticism because of inevitable false positive markers and increased reading times. Therefore, use-case specific enhanced visualization is regarded as a possibly more practical alternative [BWL*05].

2. Approach

The approaches for both use cases described below share very similar algorithms, but are adapted to the specific needs, respectively. In particular, optimal nodule detection by gradual vessel suppression requires the opacity to *decrease* with local structure size (i.e. length), whereas optimal visualization of emphysematic lung bullae requires the opacity to *increase* with structure size. The size/length of the structure at a given location $\mathbf{x}$ is estimated independently for each voxel in the following way (similar to [WKK10]): A number of search rays is cast out in 3D into N isotropically distributed directions $\hat{\mathbf{r}}_i$ (Fig. 1). The intensities are sampled along each ray i with a fixed step size dr until the intensity drops below a threshold T_{low} (use case 1) or exceeds a threshold T_{high} (use case 2). Then, from all ordered ray lengths r_i a characteristic size/length is derived corresponding to a certain percentile.

2.1. Use Case 1: Gradual Vessel Suppression

We aim to reduce the opacity of elongated structures (vessels) so that comparatively shorter structures (nodules) are

DOI: 10.2312/conf/EG2013/short/073-076

implicitly standing out more clearly. For the termination of the search rays, it is essential that the threshold T_{low} is determined individually for each voxel because neither the vessels nor the nodules have a characteristic value but are rather distributed over a wide dynamic range. We define the local $T_{low} = 0.9 \cdot I(\mathbf{x})$ as slightly below the intensity $I(\mathbf{x})$ of the center voxel in order to allow for a certain noise deviation. From all ray lengths r_i the longest is adopted as the estimation for the local structure length $r(\mathbf{x})$. Then the local structure length $r(\mathbf{x})$ is converted into an opacity $O(\mathbf{x})$ in a simple linear fashion:

$$O(\mathbf{x}) = \max\{0,\ 1 - r(\mathbf{x})/R_{\max}\}$$

where $R_{\max}$ can be changed interactively by the user in order to achieve different levels of suppression (Fig. 4). Finally, the size-based opacity $O(\mathbf{x})$ is multiplied with the original intensity $I(\mathbf{x})$ and used in a standard Maximum Intensity Projection (MIP) or Direct Volume Rendering (all renderings in this paper are MIPs).

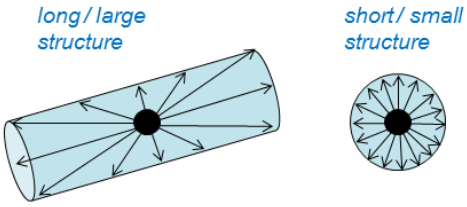

Figure 1: *Estimation of local structure size by isotropic search rays (3D).*

2.2. Use Case 2: Differentiation between Bullous versus Diffuse Emphysema

For emphysema it is common to use a certain fixed Hounsfield threshold T_{Em} below which voxels are considered emphysematic [BWL01, MZM*05]. Therefore, a standard visualization is an inverse MIP, showing low intensities most prominently. This yields a good overview over low attenuation voxels, but is not helpful in discriminating between bullous and diffuse subtypes of emphysema. Emphysematic bullae are large continuous volumes of such low attenuation voxels. Again, we estimate their size individually for each voxel by casting out search rays in 3D with a threshold $T_{high} = T_{Em}$. In contrast to a computationally more efficient connected component analysis, this has the crucial advantage that the bullae contours do not have to be strictly closed (Fig. 2). From the ordered list of ray lengths r_i we take the characteristic bulla radius r_B corresponding to the 80%-quantile. In that way, overly long rays at broken contours as well as short rays towards a nearby contour are neglected, and a robust radius estimation is achieved. We have found that the visual cues are preferable when not all low-attenuation voxels are mapped into the bulla rendering, but only the bulla contour voxels identified by the search ray termination points. These contour voxels are then multiplied with an opacity proportional to the estimated bulla radius r_B, and subjected to a standard mean projection along the viewing direction. The resulting bulla image is then coded in one specific color and superimposed onto the standard inverse MIP in another color, allowing simultaneous appraisal of the diffuse as well as the bullous component (Fig. 3).

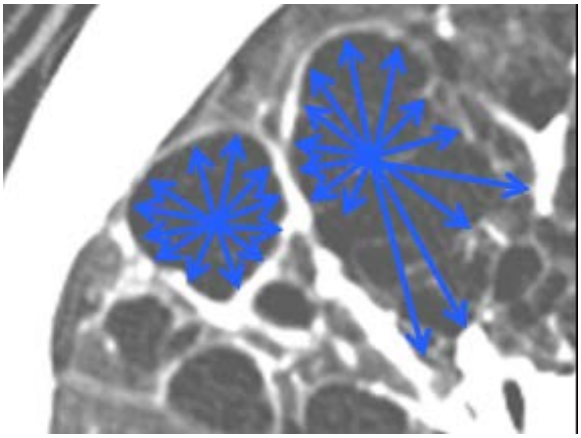

Figure 2: *Robust estimation of bulla size by search rays.*

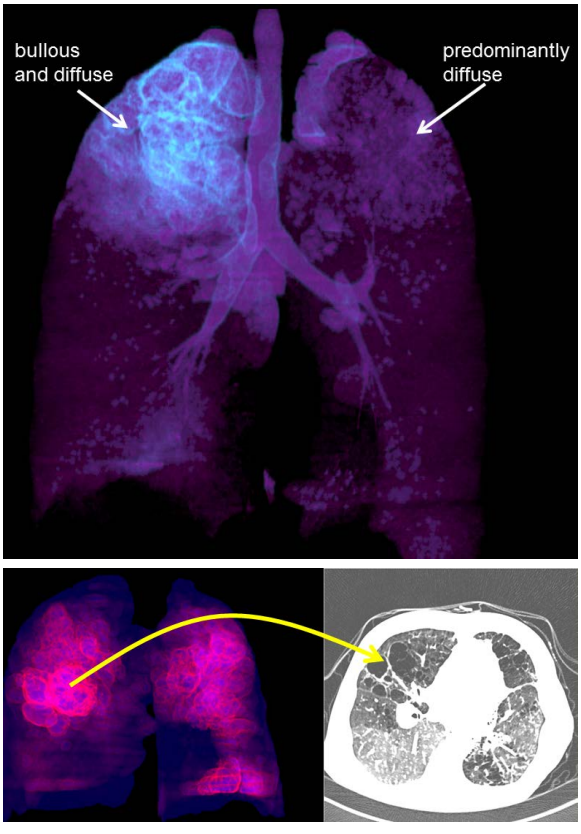

Figure 3: *Bullous and diffuse emphysematic regions.*

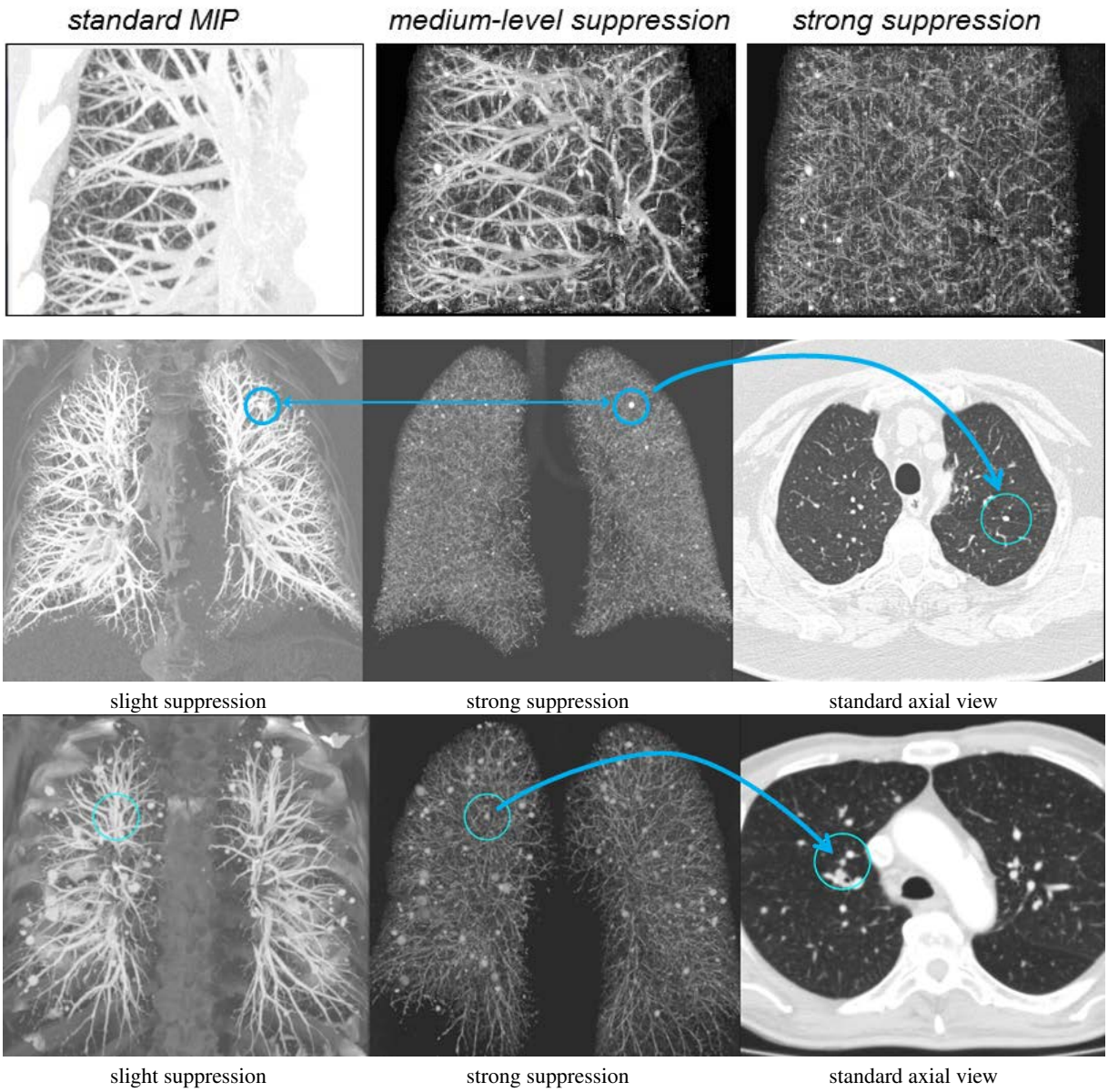

Figure 4: *Top row: Detail view. The degree of size-based suppression can be interactively changed and reveals small nodules no longer occluded by larger vessels, thorax wall and bones.*
Middle and bottom row: Clinical usage as a quick overview over nodule status and navigational aid; mouse-click refers to the corresponding location in normal slice-wise viewing for further inspection.
Note that no prior segmentation of the lung or vessels is required.
To achieve high quality renderings we have used a high number of rays $N \approx 400$*, a small radial step size* $dr \approx 0.5$ *vox, and clamped the value of* T_{low} *at* $\leq$ *bone level. Precomputation of the structure size volume requires ca. 15 sec on a NVIDIA Quadro 5000 (CUDA implementation), the change of the suppression degree is then at interactive speed.*

3. Clinical Use

The enhanced renderings are not meant to replace, but to complement the normal slice-wise viewing. They serve as a quick overview, printable key image for reporting, and navigational aid for efficient inspection of points of interest in the huge 3D image volume. For practical use, it is essential that

- ▷ the user can interactively change the degree of vessel suppression (Fig. 4, top row) or bulla enhancement,
- ▷ the rendering is linked to the original image slice such that a mouseclick immediately reveals the origin of an apparent anomaly for further inspection (Fig. 3 and 4, middle and bottom row).

Figure 4 illustrates that the interactive gradual vessel suppression allows to assess very quickly whether none, few, or many nodules are present, what their size distribution is (which has implications of their malignancy likelihood), and reveals also quite minuscule nodules hidden between vessels of equal density and diameter.

For COPD appraisal, the composite of standard and size-based rendering (Fig. 3) allows a quick overview if and to what extent emphysema is present, whether the diffuse or bullous component is predominant, and yields efficient navigation per mouse-click to diseased tissue regions.

4. Conclusions

We have presented two medical use cases for chest CT screening where size-based rendering can add clinical value to standard visualization techniques. Size-based rendering, relying on analysis of an extended local neighborhood, is computationally more expensive than rendering of pre-segmented objects or rendering of purely local features (e.g. intensities, gradients, or curvatures). However, its principal advantage is that is does not require any prior segmentations which might be erroneous and thus cause rendering artifacts or even compromise the truth of the rendering. The strictly voxelwise, curiously simple search ray algorithm yields high quality renderings which are understood intuitively by clinicians. The relevance of the use cases is evident in view of the enormous interest in lung cancer screening with CT after recent results in mortality reduction [Nat11]. Nevertheless, potential sensitivities to critical rendering parameters have to be investigated further, and a thorough validation by virtue of multi-observer studies is necessary.

Acknowledgment: The author wish to thank Ekta Dharaiya, Mark Rabotnikov, Amnon Steinberg, Yang Wang (Philips Healthcare Cleveland, Haifa, Peking), and Shiyuan Liu and Li Fan (Shanghai Changzheng Hospital) for providing clincial images and fruitful discussions.

References

[BWL01] BLECHSCHMIDT R. A., WERTHSCHÜTZKY R., LÖRCHER U.: Automated CT image evaluation of the lung - a morphology based concept. *IEEE Trans. Med. Imaging 20*, 5 (2001), 434–442. 2

[BWL*05] BÜLOW T., WIEMKER R., LORENZ C., RENISCH S., BLAFFERT T.: A method for lung nodule visualization from multi-slice CT data. In *Computer Assisted Radiology and Surgery (CARS)* (2005). 1

[CM08] CORREA C., MA K.-L.: Size-based transfer functions: A new volume exploration technique. *IEEE Transactions on Visualization and Computer Graphics 14* (2008), 1380–1387. 1

[Coc12] COCHE E.: Advances and perspectives in lung cancer imaging using multidetector row computed tomography. *Expert Rev Anticancer Ther 12*, 10 (2012), 1313–1326. 1

[HFRS*08] HADWIGER M., FRITZ L., REZK-SALAMA C., HÖLLT T., GEIER G., PABEL T.: Interactive volume exploration for feature detection and quantification in industrial CT data. *IEEE Trans Vis Comput Graph 14*, 6 (2008), 1507–1514. 1

[MJR08] MEYER H., JURAN R., ROGALLA P.: SoftMip: a novel projection algorithm for ultra-low-dose computed tomography. *J Comput Assist Tomogr 32*, 3 (2008), 480–4. 1

[MZM*05] MURA M., ZOMPATORI M., MUSSONI A., FASANO L., PACILLI A., FERRO O., SCHIAVINA M., FABBRI M.: Bullous emphysema versus diffuse emphysema: a functional and radiologic comparison. *Respir Med 99*, 2 (2005), 171–8. 2

[Nat11] NATIONAL LUNG SCREENING TRIAL RESEARCH TEAM: Reduced lung-cancer mortality with low-dose computed tomographic screening. *N Engl J Med 365*, 5 (2011), 395–409. 1, 4

[PB07] PREIM B., BARTZ D.: *Visualization in Medicine. Theory, Algorithms, and Applications*. Morgan Kaufmann, 2007. 1

[PSW*07] PELOSCHEK P., SAILER J., WEBER M., HEROLD C. J., PROKOP M., SCHAEFER-PROKOP C.: Pulmonary nodules: sensitivity of maximum intensity projection versus that of volume rendering of 3D multidetector CT data. *Radiology 243*, 2 (May 2007), 561–569. 1

[SHA*07] SPITZ M., HONG W., AMOS C., WU X., SCHABATH M., DONG Q., SHETE S., ETZEL C.: A risk model for prediction of lung cancer. *J Natl Cancer Inst 99*, 9 (2007), 715–26. 1

[SWB*00] SATO Y., WESTIN C.-F., BHALERAO A., NAKAJIMA S., SHIRAGA N., TAMURA S., KIKINIS R.: Tissue classification based on 3D local intensity structure for volume rendering. *IEEE Trans Vis Comput Graph 6*, 2 (2000), 160–180. 1

[WDB12] WIEMKER R., DHARAIYA E., BÜLOW T.: Hesse rendering for computer-aided visualization and analysis of anomalies at chest CT and breast MR imaging. *Radiographics 32*, 1 (2012), 289–304. 1

[WK09] WESARG S., KIRSCHNER M.: Structure size enhanced histogram. In *Bildverarbeitung für die Medizin* (2009), pp. 16–20. 1

[WKB*12] WIEMKER R., KLINDER T., BERGTHOLDT M., MEETZ K., CARLSEN I., BÜLOW T.: A radial structure tensor and its use for shape-encoding medical visualization of tubular and nodular structures. *IEEE Trans Vis Comput Graph* (2012). 1

[WKK10] WESARG S., KIRSCHNER M., KHAN M.: 2D histogram based volume visualization: combining intensity and size of anatomical structures. *Int J CARS 5* (2010), 655–666. 1